Time-domain simulation of second-order irregular wave diffraction based on a hybrid water wave radiation condition

G. Xu [a,c], A.M.S. Hamouda [a,*], B.C. Khoo [b]

[a] *Department of Mechanical and Industrial Engineering, Qatar University, Qatar*
[b] *Department of Mechanical Engineering, National University of Singapore, Singapore*
[c] *School of Naval Architecture and Ocean Engineering, Jiangsu University of Science and Technology, China*

ARTICLE INFO

ABSTRACT

A time-domain second-order method is presented to simulate three-dimensional wave–body interaction. In the approach, Taylor series expansions are applied to the free surface boundary conditions, and a Stokes perturbation procedure is then used to establish the corresponding boundary value problem at first order and second order on the time-independent surfaces. A constant boundary element method, based on a Rankine source, is used to calculate the wave field at each time step. A proposed hybrid radiation condition, which is a combination of the multitransmitting formula and the damping zone, is studied to minimize the wave reflection, a stable integral form of the free-surface boundary condition is used to update the velocity potential on the free surface, and an auxiliary function is used to calculate high-order derivatives. The proposed model is first validated by linear irregular wave diffraction and is then applied to compute the second-order irregular Stokes wave diffraction with three wave components. It is shown that long time simulation can be performed with stability and accuracy and that the model can be used to simulate nonlinear irregular wave–structure interaction.

1. Introduction

It is well known that second-order effects may be important for the nonlinear hydrodynamic problem arising in many aspects of ocean engineering. Numerous studies have been published to date [1–7]. However, for the time-domain numerical simulation, the solution generally requires truncation of the fluid domain at some finite distance. There is no exact nonreflecting boundary condition for the truncated domain surface. For a long time simulation, an appropriate and effective radiation condition should be imposed on the so-called artificial boundary to minimize any wave reflection. This is a common problem faced in the numerical modeling of wave propagation. Various techniques have been developed to satisfy the radiation condition. Newman [8] introduced a theoretical method to absorb reflected waves on the sides of the closed basin for a linear potential; however, it is hard to apply the method to the analysis of the nonlinear case. Orlanski's method [9] and the absorbing beach scheme [10] have generally been implemented to model the open boundary. However, Orlanski's method may produce incorrect phase velocity if the mesh size is not sufficiently small near the open boundary. Clément [11] proposed a coupling method (piston-beach hybrid absorber) to absorb the wave, whereas Boo [12] used a numerical scheme which combines an absorbing beach and the stretching technique [13] to simulate the open boundary. Wang and Wu [7] imposed a radiation condition through a combination of the damping zone and the Sommerfeld–Orlanski equation. Clamond et al. [14] introduced a numerical beach to damp the (scaled)

---

* Corresponding author. Tel.: +974 55360976; fax: +974 44034122.
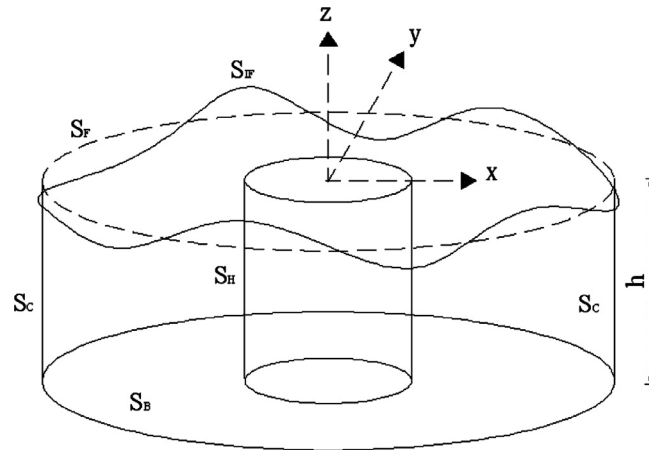 *E-mail address:* hamouda@qu.edu.qa (A.M.S. Hamouda).

Fig. 1. Definition sketch.

tangential velocity at the free surface, with all the frequencies being damped with the same intensity. However, the efficiency of the damping zone method strongly depends on the ratio between the width of the beach and the length of the wave.

To find a more efficient and effective radiation condition to deal with the nonlinear irregular wave problem in the time domain, a multitransmitting formula (MTF) [15] used as the radiation condition for a water wave field is introduced. It has already been used in a finite element method to achieve the nonreflecting condition in the field of seismology by Liao [16], and has proven to be effective in the simulation of the earthquake waves. On the basis of the MTF method, the values of the diffracted velocity potential at certain positions (named the "transmitting layers") in the inner fluid domain [17] are obtained at each time step. Then the velocity potentials on the artificial boundary at the present time step can be formulated by potentials at prior time steps on the transmitting layers. In the MTF method, an artificial wave velocity is used to replace the actual wave velocity. Usually, it is not necessary to make the artificial wave velocity equal to the actual wave velocity. As a result, the flexibility of the method is very useful for dealing with the irregular wave problem. However, the MTF method can transmit waves only out of the artificial boundary effectively when the artificial wave velocity is in a certain range of the given actual wave velocity. Numerical tests in this work will show that a weak wave reflection from the open boundary is usually nonnegligible for irregular wave diffraction by the MTF method. As such, an improvement in treating this radiation condition becomes essential. On examining a variety of approaches, one finds that the hybrid method with a damping zone is an effective approach to eliminate the problem. Fairly similar findings have also been shown by Xu [18], Duan and Zhang [19], and Zhang and Duan [17].

Theoretically, numerical calculation based on the boundary element method can benefit much from the MTF approach compared with the damping zone approach [17]. Firstly, only one coefficient, named the "artificial velocity," needs to be considered in the MTF. The artificial velocity is a rough estimation of the actual wave velocity, which is usually fairly easy to obtain. Secondly, fewer elements are needed to be distributed on the fluid boundary in comparison with the damping zone. Thirdly, the numerical implementation is simpler than that of other radiation conditions. Finally, extension to nonlinear problems is possible—for example, second-order nonlinear [18,20,21] and fully nonlinear [19] problems. The MTF method has also been successfully used for simulation of harmonic wave radiation and diffraction [22,23] and irregular wave diffraction [24]. The first attempt to simulate second-order irregular wave diffraction was published by Xu and Hamouda [25]. In their article, only the hybrid water wave radiation condition to simulate the nonlinear wave–structure interaction was mentioned; however, the convergent study of artificial water wave velocity applied in the MTF method and the hybrid condition was not presented, especially for the irregular wave diffraction cases. In the present work, a detailed expression of two auxiliary functions and the integral form of the free-surface boundary condition is introduced where the values of the velocity potential on the free surface are easily estimated at each time step, and which shows excellent stabilities in our various numerical simulations for both linear and second-order cases. On the basis of the linear water wave diffraction theory, the stability of the MTF method has been studied. Our hybrid model is first verified by the linear irregular wave diffraction and the results obtained are compared with the frequency-domain solution. We find the effective length of the damping zone which suffices for the hybrid method. Next, the model is applied to the time-domain computation of the second-order Stokes wave diffraction of a bottom-mounted circular cylinder at finite water depth and the second-order irregular Stokes wave diffraction of a truncated cylinder at infinite water depth for both the high-frequency and the low-frequency wave–structure interaction cases. The model has been found to be accurate and efficient.

2. Mathematical formulation

The reference system of Cartesian coordinates is defined with the (x, y) plane coinciding with the still water surface S_F and z pointing vertically upward from the still water level as shown in Fig. 1. The body located at the center of the domain is rigid and fixed, and the instantaneous wetted body surface is denoted by S_H and its unit normal vector directed outward from the fluid region is denoted by $\boldsymbol{n}$. The seabed S_B is assumed to be horizontal along the plane at $z=-h$. Let t denote time and η be the

elevation of instantaneous free surface S_{IF} relative to the still water surface S_F. An artificial boundary S_C is introduced, which divides the fluid domain into the inner and outer regions. The incident waves are two-dimensional in the x-z plane and are progressive in the positive x direction.

As per the usual assumption of potential flow theory, the fluid is assumed to be incompressible and inviscid and the flow is assumed to be irrotational. Then the fluid motion can be described by a velocity potential ϕ which satisfies Eq. (1) within the fluid domain Ω_f,

$$\nabla^2 \phi = 0 \quad \text{in } \Omega_f; \tag{1}$$

and subject to the following boundary conditions:

$$\partial \phi / \partial n = 0 \quad \text{on } S_H, \tag{2}$$

$$\frac{\partial \phi}{\partial z} - \frac{\partial \eta}{\partial t} - \frac{\partial \phi}{\partial x}\frac{\partial \eta}{\partial x} - \frac{\partial \phi}{\partial y}\frac{\partial \eta}{\partial y} = 0 \quad \text{on } S_{IF}, \tag{3}$$

$$\frac{\partial \phi}{\partial t} + g\eta + \frac{1}{2}|\nabla \phi|^2 = 0 \quad \text{on } S_{IF}, \tag{4}$$

$$\partial \phi / \partial z = 0 \quad \text{on } S_B, \tag{5}$$

where g is the acceleration due to gravity. Eqs. (3) and (4) correspond to the kinematic and dynamic free surface boundary conditions, respectively. In addition, a nonreflecting boundary condition is imposed on the artificial boundary (S_C) as indicated in Fig. 1. This will be discussed further in Sections 2.2 and 2.3.

On the basis of the second-order theory for the weakly nonlinear problem, Eqs. (3) and (4) can be satisfied on the still water surface ($z = 0$) through a Taylor expansion as shown in Eqs. (6) and (7):

$$\left(\frac{\partial \phi}{\partial z} - \frac{\partial \eta}{\partial t} - \frac{\partial \phi}{\partial x}\frac{\partial \eta}{\partial x} - \frac{\partial \phi}{\partial y}\frac{\partial \eta}{\partial y}\right)\Big|_{z=0} + \eta \frac{\partial}{\partial z}\left(\frac{\partial \phi}{\partial z} - \frac{\partial \eta}{\partial t} - \frac{\partial \phi}{\partial x}\frac{\partial \eta}{\partial x} - \frac{\partial \phi}{\partial y}\frac{\partial \eta}{\partial y}\right)\Big|_{z=0} + \cdots = 0 \quad \text{on } z = 0, \tag{6}$$

$$\left(\frac{\partial \phi}{\partial t} + g\eta + \frac{1}{2}|\nabla \phi|^2\right)\Big|_{z=0} + \eta \frac{\partial}{\partial z}\left(\frac{\partial \phi}{\partial t} + g\eta + \frac{1}{2}|\nabla \phi|^2\right)\Big|_{z=0} + \cdots = 0 \quad \text{on } z = 0. \tag{7}$$

Correspondingly, we can write:

$$\phi = \varepsilon \phi^{(1)} + \varepsilon^2 \phi^{(2)} + \cdots, \tag{8}$$

$$\eta = \varepsilon \eta^{(1)} + \varepsilon^2 \eta^{(2)} + \cdots, \tag{9}$$

where ε is a perturbation parameter which is usually related to the wave slope and the superscripts 1 and 2 denote the first-order and second-order components of the velocity potential, respectively. The components are further split into $\phi^{(k)} = \phi_I^{(k)} + \phi_D^{(k)}$, where $\phi_I^{(k)}$ are the known incident potentials and $\phi_D^{(k)}$ are the unknown diffracted potentials. Substituting Eqs. (8) and (9) into Eqs. (1)–(5), we find the governing equations for $\phi_D^{(k)}$ ($k = 1, 2$) become:

$$\nabla^2 \phi_D^{(k)} = 0 \text{ in } \Omega_f^{(0)}, \tag{10}$$

where $\Omega_f^{(0)}$ is the fixed fluid domain below $z = 0$.

The boundary conditions based on the order of ε are shown in Eqs. (11)–(13):

$$\frac{\partial \phi_D^{(k)}}{\partial n} = -\frac{\partial \phi_I^{(k)}}{\partial n} \text{ on } S_H^{(0)}, \tag{11}$$

$$\frac{\partial^2 \phi_D^{(k)}}{\partial t^2} + g\frac{\partial \phi_D^{(k)}}{\partial z} = f^k \text{ on } S_F, \tag{12}$$

$$\frac{\partial \phi_D^{(k)}}{\partial z} = 0 \text{ on } S_B, \tag{13}$$

where $S_H^{(0)}$ is the body surface below the still water level. The terms f^k in these equations are described in Eqs. (14) and (15):

$$f^1 = 0, \tag{14}$$

$$f^2 = -\left(\frac{\partial^2 \phi_I^{(2)}}{\partial t^2} + g\frac{\partial \phi_I^{(2)}}{\partial z}\right) - 2\nabla \phi^{(1)} \cdot \nabla\left(\frac{\partial \phi^{(1)}}{\partial t}\right) + \frac{1}{g}\frac{\partial \phi^{(1)}}{\partial t} \cdot \frac{\partial}{\partial z}\left(\frac{\partial^2 \phi^{(1)}}{\partial t^2} + g\frac{\partial \phi^{(1)}}{\partial z}\right). \tag{15}$$

The hydrodynamic forces F_j on the body can be calculated by integration of the pressure over its wetted surface $S_H^{(0)}$. For the second-order problem, the equation can be written as [4,7]:

$$\mathbf{F} = -\rho \iint_{S_H^{(0)}} \left(\frac{\partial \phi^{(1)}}{\partial t} + \frac{\partial \phi^{(2)}}{\partial t} + \frac{1}{2} \left| \nabla \phi^{(1)} \right|^2 + gz \right) n \, ds + \frac{1}{2} \rho g \iint_{w_0} (\eta^{(1)})^2 n \, dw, \tag{16}$$

where w_0 is the mean waterline. The last term in Eq. (16) is due to the variation of S_H with the water surface. To compare the time-domain results with frequency-domain results, Eq. (16) can be further split into three components, as shown in Eq. (17):

$$\mathbf{F} = \mathbf{F}^{(1)} + \mathbf{F}^{(2)} + \mathbf{F}_0, \tag{17}$$

where $\mathbf{F}^{(1)}$, $\mathbf{F}^{(2)}$, and $\mathbf{F}_0$ are the first-order oscillatory wave force at the incident wave frequency, the second-order oscillatory wave force at twice the wave frequency, and the second-order steady drift force, respectively. The second-order oscillatory wave force is composed of two components $\mathbf{F}^{(21)}$ and $\mathbf{F}^{(22)}$. The expressions for $\mathbf{F}^{(1)}$, $\mathbf{F}^{(21)}$, $\mathbf{F}^{(22)}$, and F_0 are given in Eqs. (18)–(21), respectively:

$$\mathbf{F}^{(1)} = -\rho \iint_{S_H^{(0)}} \frac{\partial \phi^{(1)}}{\partial t} n \, ds, \tag{18}$$

$$\mathbf{F}^{(21)} = -\frac{1}{2} \rho \iint_{S_H^{(0)}} \left| \nabla \phi^{(1)} \right|^2 n \, ds + \frac{1}{2} \rho g \iint_{w_0} (\eta^{(1)})^2 n \, dw - \mathbf{F}_0, \tag{19}$$

$$\mathbf{F}^{(22)} = -\rho \iint_{S_H^{(0)}} \frac{\partial \phi^{(2)}}{\partial t} n \, ds, \tag{20}$$

$$\mathbf{F}_0 = -\frac{1}{2} \rho \left\langle \iint_{S_H^{(0)}} \left| \nabla \phi^{(1)} \right|^2 n \, ds \right\rangle + \frac{1}{2} \rho g \left\langle \int_{w_0} (\eta^{(1)})^2 n \, dw \right\rangle. \tag{21}$$

2.1. Integral form of the free-surface boundary condition

Researchers have adopted various schemes to evolve the free-surface conditions—for example, higher-order explicit methods (e.g., the Runge–Kutta method) and multistep methods (e.g., the Adams–Bashforth–Moulton method)—so that at each time step the velocity potential on the free-surface can be obtained as the known quantity. However, in this work, we rewrite the boundary conditions in an integral form and use an integral method as the time-integration scheme [17,18]; this has given rise to excellent stabilities in our numerical tests.

We integrate each term in Eqs. (12), (14), and (15) twice with respect to time in order to obtain the explicit form of $\phi_D^{(k)}$. One example relationship is shown for illustration as presented in Eq. (22):

$$\int_0^\tau d\tau_1 \int_0^{\tau_1} f(t) \, dt = \int_0^\tau f(t) \, dt \int_t^\tau d\tau_1 = \int_0^\tau (\tau - t) f(t) \, dt. \tag{22}$$

The diffracted velocity potential ϕ_D on the free surface given in Eq. (12) can be obtained as Eqs. (23) and (24) [26]:

$$\phi_D^{(1)}(p, t) = \phi_D^{(1)}(p, 0) + \int_0^t \frac{\partial \phi_D^{(1)}(p, 0)}{\partial \tau} d\tau - g \int_0^t (t - \tau) \frac{\partial \phi_D^{(1)}(p, \tau)}{\partial z} d\tau, \tag{23}$$

$$\phi_D^{(2)}(p, t) = \phi_D^{(2)}(p, 0) + \int_0^t \frac{\partial \phi_D^{(2)}(p, 0)}{\partial \tau} d\tau$$

$$- g \int_0^t (t - \tau) \frac{\partial \phi_D^{(2)}(p, \tau)}{\partial z} d\tau - \int_0^t \left| \nabla \phi_I^{(1)}(p, 0) \right|^2 d\tau$$

$$- \int_0^t \left| \nabla \phi^{(1)}(p, \tau) \right|^2 d\tau + \int_0^t \left| \nabla \phi^{(1)}(p, 0) \right|^2 d\tau + \int_0^t \left| \nabla \phi_I^{(1)}(p, \tau) \right|^2 d\tau$$

$$+ \frac{1}{g} \int_0^t (t - \tau) \frac{\partial \phi^{(1)}(p, \tau)}{\partial \tau} \cdot \frac{\partial}{\partial z} \left(\frac{\partial^2 \phi^{(1)}(p, \tau)}{\partial \tau^2} + g \frac{\partial \phi^{(1)}(p, \tau)}{\partial z} \right) d\tau$$

$$- \frac{1}{g} \int_0^t (t - \tau) \frac{\partial \phi_I^{(1)}(p, \tau)}{\partial \tau} \cdot \frac{\partial}{\partial z} \left(\frac{\partial^2 \phi_I^{(1)}(p, \tau)}{\partial \tau^2} + g \frac{\partial \phi_I^{(1)}(p, \tau)}{\partial z} \right) d\tau. \tag{24}$$
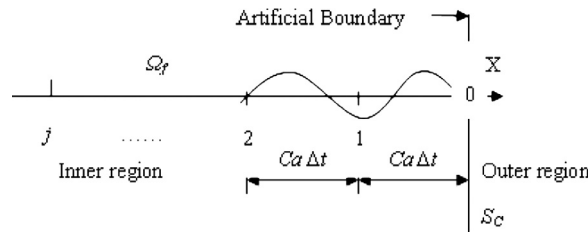
Fig. 2. Radiation condition on the artificial boundary.

The trapezoidal numerical integral method is used for the integration terms, and the solutions for $\frac{\partial^3 \phi_D^{(1)}(p,\tau)}{\partial z \partial \tau^2}$ and $\frac{\partial^2 \phi_D^{(1)}(p,\tau)}{\partial z^2}$ can be found in Appendixes A and B, respectively.

2.2. MTF on an artificial boundary

Liao [15,16] has described and provided a general expression for one-way wave propagation and developed a system of local nonreflecting boundary conditions using space-time extrapolation. Its original aim is to deal with the propagation of an earthquake wave out of the artificial boundary.

The MTF method for diffracted velocity potential ϕ_D (hereinafter referred to as ϕ in the MTF) in a water wave field will be introduced below. Let the x-axis be the normal to S_C and point toward the outer region of the model, as shown in Fig. 2. Suppose that the intersection point 0 is on the artificial boundary under consideration and that j are the points away from point 0 along its normal vector in the inner region. The distance between point j and point 0 is $jC_a\Delta t$ along the normal vector to the point 0 in the inner region, where C_a is an artificial wave speed and Δt is the time interval.

The Nth-order nonreflecting radiation condition on S_C can be written as:

$$\varphi_0^{p+1} = \sum_{j=1}^{N} (-1)^{j+1} C_j^N \varphi_j^{p+1-j}, \tag{25}$$

where integer p represents the time level and N is the order of the MTF method. The binomial coefficients C is described in Eq. (26):

$$C_j^N = \frac{N!}{(N-j)!\,j!}. \tag{26}$$

In this work, the second-order MTF method ($N = 2$) will be considered. So Eq. (25) can be written as:

$$\phi_0^{p+1} = 2\phi_1^p - \phi_2^{p-1}, \tag{27}$$

where the subscript 0 represents the point on the artificial boundary, and 1 and 2 are, respectively, the points which are $C_a\Delta t$ and $2C_a\Delta t$, away from point 0 along its normal vector in the inner region.

To eliminate the effect of the frequencies, which are near to and including zero, a constant value γ_2 (additional factor) is suggested. As such, Eq. (27) can be further written as:

$$\varphi_0^{p+1} = \frac{2}{1+\gamma_2}\varphi_1^p - \frac{1}{(1+\gamma_2)^2}\varphi_2^{p-1}. \tag{28}$$

On the basis of Eq. (28), at each time step, the velocity potential on the artificial boundary can be obtained from those in the fluid domain at previous time steps. Then, the MTF method can be used to solve the water wave problems with the boundary element method, as shown in Fig. 3. For more details on the MTF method applied to the earthquake wave and water wave fields, see Liao [16], Xu [18], and Zhang and Duan [17].

2.3. Hybrid method with a damping zone

The MTF method can transmit the wave out of the artificial boundary effectively only when the artificial wave velocity C_a is in the prescribed range [16–18]. Thus, another appropriate radiation condition should be coupled with the MTF on the artificial boundary to minimize the wave reflection when we simulate wave–body interaction for an irregular wave [17–19]. Here, we will use a combination of the MTF method and damping zone method (i.e., a hybrid method), as shown in Fig. 4. The damping zone method adopted is similar to the one used by Sclavounos and Nakos [27]. We rewrite Eq. (12) as:

$$\frac{\partial^2 \phi_D^{(k)}}{\partial t^2} + g\frac{\partial \phi_D^{(k)}}{\partial z} = f^k + 2g\mu\eta_D^{(k)} - \mu^2\phi_D^{(k)}, \tag{29}$$
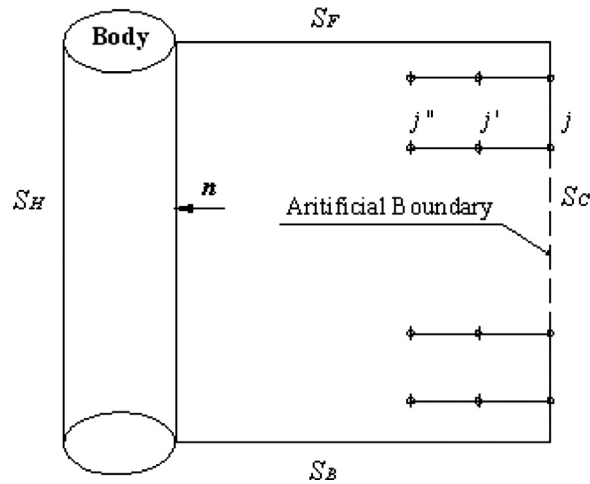
Fig. 3. Multitransmitting formula (MTF) for an artificial boundary in the boundary element method.
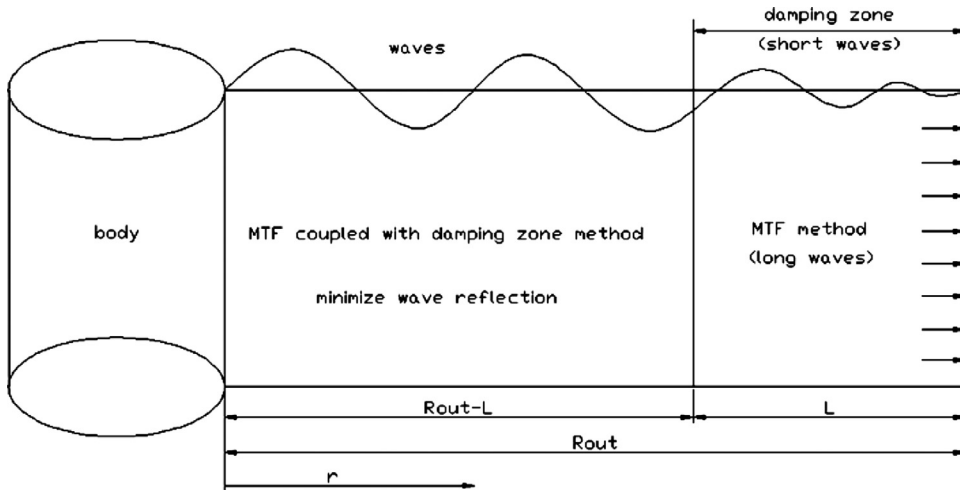

Fig. 4. The concept of the MTF and damping zone (DZ) method.

where μ is the damping coefficient given by:

$$\mu(r) = 3\mu_0 \frac{[r - (R_{\text{out}} - L)]^2}{L^3}, \qquad (R_{\text{out}} - L) < r < R_{\text{out}}, \tag{30}$$

where L is the length of the damping zone and r is the distance for the point under consideration to the nearest surface of the cylinder, as shown in Fig. 4. The damping zone starts from the edge of an inner free-surface boundary $r = R_{\text{out}} - L$ and ends at the outer free-surface boundary $r = R_{\text{out}}$. μ_0, used in Eq. (30), is a constant value to control the strength of the damping coefficient.

2.4. Integral equation and boundary element discretization

The diffracted velocity potential on the surfaces of the fluid domain is expressed by the following boundary integral equation based on the three-dimensional form of Green's theorem:

$$\iint\limits_{S} \left[G \cdot \frac{\partial \phi_{\text{D}}^{(k)}(q, \tau)}{\partial n_q} - \phi_{\text{D}}^{(k)}(q, \tau) \frac{\partial G}{\partial n_q} \right] ds_q = 2\pi \phi_{\text{D}}^{(k)}(p, \tau). \tag{31}$$

Here $p(x,y,z)$ is a field point and $q(\xi,\eta,\zeta)$ is a source point on the surface S of the domain and $G(p,q)$ is the Green's function. For cases in which the seabed is horizontal, a Green's function which contains the fundamental solution of the Laplace equation and its images can be chosen to account for the symmetry about the seabed. In this manner, S_B can be excluded from the surface S,

Table 1
Basic parameters for linear incident wave diffraction.

k	λ (m)	A	C_x (m/s)	R_{out}	a	h
2.0	3.14	1	2.215	λ	1.0	λ

and the mesh on the seabed does not need to be generated. The Green's function is presented in Eq. (32):

$$G(p, (q, q')) = \sum_{k=1}^{2} \frac{1}{r_k}, \tag{32}$$

where r_k is the distance between the field point and source point. q' is the image of q about the seabed. Thus, r_k is given by Eqs. (33) and (34):

$$r_1{}^2 = (x - \xi)^2 + (y - \eta)^2 + (z - \zeta)^2, \tag{33}$$

$$r_2{}^2 = (x - \xi)^2 + (y - \eta)^2 + (z + 2h + \zeta)^2. \tag{34}$$

Next, Eq. (31) can be solved by a numerical procedure in which S_F, $S_H^{(0)}$, and S_C are discretized into a finite number of panels. The corresponding values of $\partial\phi_D/\partial n$ and ϕ_D are applied at the centroid of the panels.

As such, Eq. (31) can be represented by Eq. (35):

$$\sum_{j=1}^{nS_H^{(0)}} D_{ij}\phi_{Djm}^{(k)} - \sum_{j=nS_H^{(0)}+1}^{nS_H^{(0)}+nS_F} S_{ij}\left(\frac{\partial\phi_D^{(k)}}{\partial n}\right)_{jm} - \sum_{j=nS_H^{(0)}+nS_F+1}^{nS_H^{(0)}+nS_F+nS_C} S_{ij}\left(\frac{\partial\phi_D^{(k)}}{\partial n}\right)_{jm}$$

$$= \sum_{j=1}^{nS_H^{(0)}} S_{ij}\left(-\frac{\partial\phi_I^{(k)}}{\partial n}\right)_{jm} - \sum_{j=nS_H^{(0)}+1}^{nS_H^{(0)}+nS_F} D_{ij}\phi_{Djm}^{(k)} - \sum_{j=nS_H^{(0)}+nS_F+1}^{nS_H^{(0)}+nS_F+nS_C} D_{ij}\phi_{Djm}^{(k)} \quad i = 1, 2, \ldots, (n S_H^{(0)} + nS_F + nS_C), \tag{35}$$

in which subscripts i and j denote the centroid of the ith and jth panels, respectively, $nS_H^{(0)}$, nS_F, and nS_C are the number of panels on S_F, $S_H^{(0)}$, and S_C, respectively, and m represents the present time step. The matrix coefficients S_{ij} and D_{ij} on the collocation point of the ith panel which are influenced by the jth panel are presented in Eqs. (36) and (37):

$$S_{ij} = \iint_{\Delta Q_j} \frac{1}{r_{ij}} dS_j + \iint_{\Delta Q_{j'}} \frac{1}{r_{ij'}} dS_{j'}, \tag{36}$$

$$D_{ij} = \begin{cases} 2\pi + \iint_{\Delta Q_{j'}} \frac{\partial}{\partial n_{j'}}\left(\frac{1}{r_{ij'}}\right) dS_{j'}, & i = j, \\ \iint_{\Delta Q_j} \frac{\partial}{\partial n_j}\left(\frac{1}{r_{ij}}\right) dS_j + \iint_{\Delta Q_{j'}} \frac{\partial}{\partial n_{j'}}\left(\frac{1}{r_{ij'}}\right) dS_{j'}, & i \neq j, \end{cases} \tag{37}$$

where ΔQ is the area of the jth panel.

3. Numerical results and discussions

3.1. Stability analysis of the MTF method based on linear wave diffraction

Before we consider the case with second-order irregular wave diffraction, the model is first validated by simulation of linear wave diffraction. The parameters for the incident wave are given in Table 1, where k is the wave number, λ is the wavelength, A is the wave amplitude, C_x is the actual wave velocity, R_{out} is the distance from the artificial boundary to the nearest structure surface, a is the radius of cylinder, and h is the water depth. The model is applied to the bottom-mounted, vertical, circular cylinder, as shown in Fig. 5.

In this section, the numerical parameters of the MTF method, such as the additional factor and the artificial wave velocity will be discussed. Firstly, the additional factor γ_2, used in Eq. (28), is investigated. The nondimensional diffracted wave potential on the body surface is presented in Fig. 6, where ka is 2.0. We can see that the additional factor ($\gamma_2 = 0$, 0.001, and 0.5) obviously affects the diffracted wave potential on the body surface, where the sampling point is located at ($x = 0.992$ m, $y = 0.087$ m, $z = -0.079$ m). We can find that the convergent result can be obtained when γ_2 is in the range [0.005, 0.05]. The same conclusion can be found when we present the hydrodynamic force acting on the cylinder, as shown in Fig. 7. We can see that the numerical solution obtained by the present model agrees well with the analytical solution [28] while γ_2 is in the prescribed range. Because of this, $\gamma_2 = 0.025$ is adopted for the rest of our simulation.
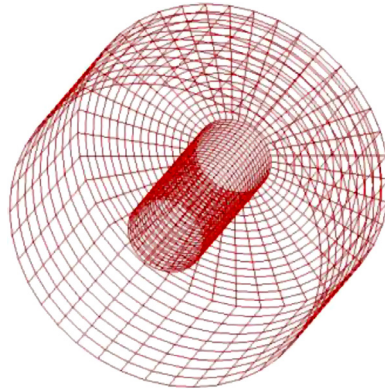
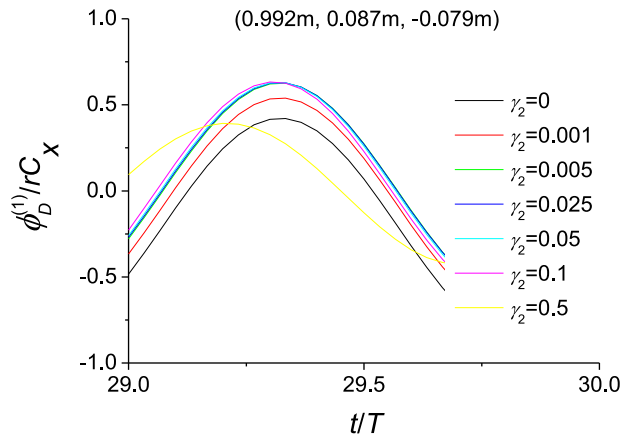**Fig. 5.** Mesh of the bottom-mounted vertical cylinder.

Fig. 6. Comparison of diffracted wave potential on the body surface ($x = 0.992$ m, $y = 0.087$ m, $z = -0.079$ m) with different γ_2 at $ka = 2.0$.
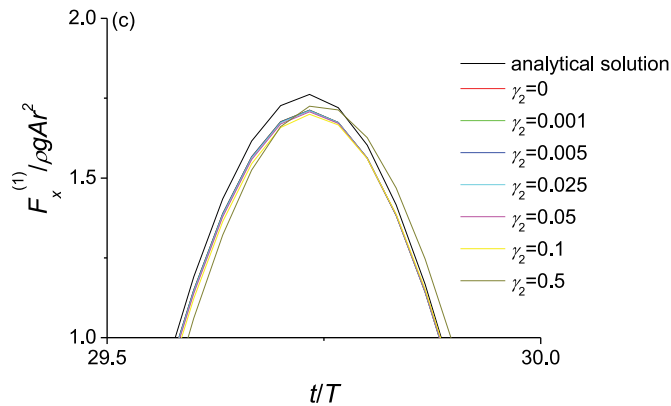

Fig. 7. Comparison of hydrodynamic force in the x direction with different values of the additional parameter γ_2 at $ka = 2.0$.

To transmit the diffracted wave out of the artificial boundary efficiently and predict the hydrodynamic force acting on the body accurately, the effect of the artificial wave velocity C_a is investigated next. Fig. 8 shows the nondimensional diffracted wave potential on the body surface for different C_a. As presented in Fig. 8, convergent results can be obtained when we set C_a to $0.6C_x$, $1.6C_x$, and $2.4C_x$. The calculated nondimensional hydrodynamic force acting on the cylinder is presented in Fig. 9. The results show that good agreement can be obtained when the artificial wave velocity C_a is taken to be close to the actual wave velocity C_x. Still, a reasonable range of C_a is applicable, which facilitates flexibility in the implementation. Usually, good agreement can be obtained when C_a is in a certain prescribed range of C_x (taken to be $C_a \in 0.6C_x$-$2.4C_x$). This suggests that we can use a different artificial wave velocity to transmit the same outgoing wave out of an artificial boundary fairly efficiently. It implies and indicates
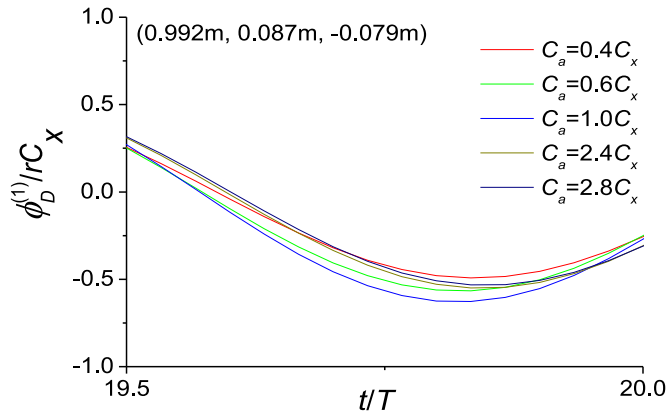
Fig. 8. Comparison of the velocity potential on the body surface at ($x = 0.992$ m, $y = 0.087$ m, $z = -0.079$ m) with different artificial wave speeds C_a
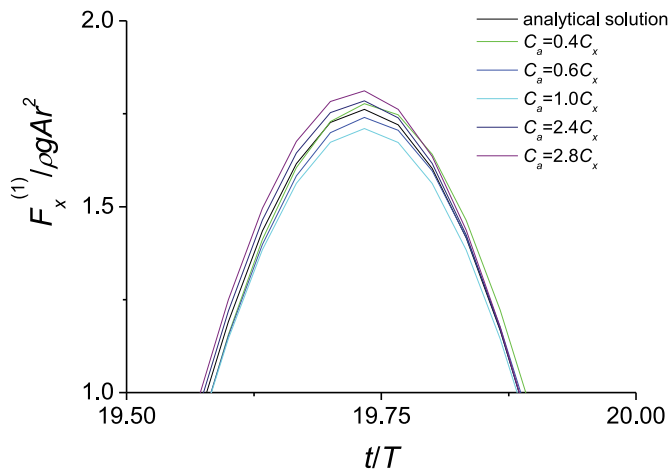

Fig. 9. Comparison of hydrodynamic force with different C_a at $ka = 2.0$.

that the present model can be used and is perhaps ideally suited for the simulation of nonlinear irregular wave diffraction in the time domain.

3.2. Linear irregular wave diffraction by the MTF method

An irregular wave system is assumed to act on the bottom-mounted cylinder. The linear irregular incident wave potential $\phi_I^{(1)}$ can be written as:

$$\phi_I^{(1)} = \sum_{i=1}^{N} \frac{gA_i}{\omega_i} \frac{\cosh[k_i(z+h)]}{\cosh(k_i h)} \sin(k_i x - \omega_i t + \varepsilon_i), \tag{38}$$

where A, ω, k, and ε are the incident wave amplitude, angular frequency, wave number, and random phase angle of wave component number i, respectively.

To investigate the linear irregular wave diffraction of a bottom-mounted vertical cylinder ($a = 7.5$ m), a sea spectrum from the International Towing Tank Conference, as shown in Fig. 10, is used to generate the irregular wave.

Here

$$S_\zeta(\omega) = \frac{A_S}{\omega^5} e^{-\frac{B}{\omega^4}} \quad (\text{m}^2/\text{s}), \tag{39}$$

where $A_S = 8.10 \times 10^{-3} g^2$ and $B = 3.11/(h_{1/3})^2$. The wave amplitude A_i can be expressed by the wave spectrum $S_\zeta(\omega)$, and is given by

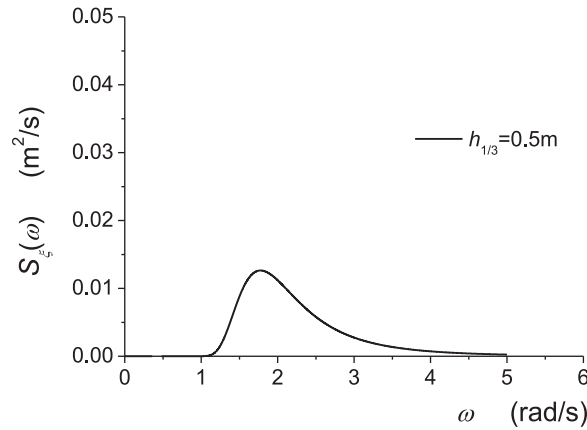$$A_i = \sqrt{2 S_\zeta(\omega_i) \Delta\omega}, \tag{40}$$

Fig. 10. Sea spectrum from the International Towing Tank Conference ($h_{1/3} = 0.5$ m).
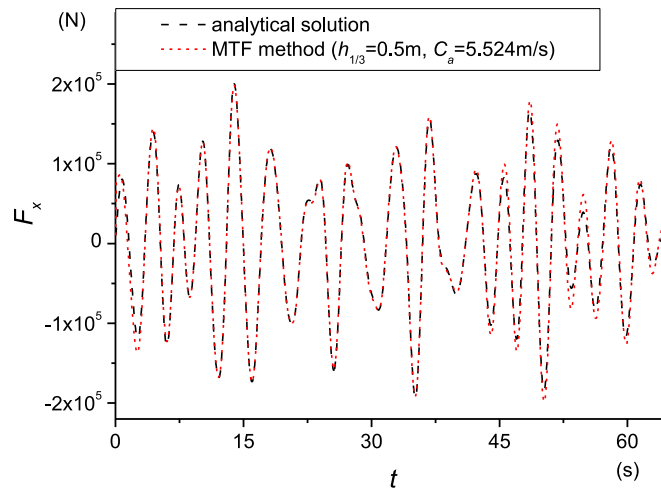

Fig. 11. Significant wave height $h_{1/3} = 0.5$ m ($\omega_{min} = 1.109$ rad/s, $\omega_{max} = 5.714$ rad/s).

Table 2
Basic parameters for linear irregular wave diffraction.

$h_{1/3}$	5 m	
ω (rad/s)	ω_{min}	ω_{max}
1% $S_{\zeta max}$	0.350	1.807
C_x (m/s)	28.0	5.4
$0.6C_x$	16.817	3.257
$1.6C_x$	44.846	8.686
$S_\zeta(\omega)_{max}$	$S_\zeta(\omega)_{max}$	
ω (rad/s)	0.562	
C_a (m/s)	17.456	

where $\Delta\omega$ is a constant difference between successive frequencies. For simplicity, the irregular wave is approximated by other regular waves in this example. In this work, the wave component is determined by the peak value $S_{\zeta max}$ of the wave spectrum. The wave components ω_i are considered when $S_\zeta(\omega_i)$ are greater than $S_{\zeta max}/100$.

The phase angles ε_i are randomly distributed between 0 and 2π, and are constant with time. The frequency of the peak value $S_{\zeta max}$ is 0.562 rad/s, whereas the significant wave height of the irregular wave is 0.5 m. In the simulation, the artificial wave velocity is equal to the actual wave velocity relative to the wave component of peak value $S_{\zeta max}$ in the wave spectrum. The basic parameters for the irregular wave diffraction are given in Table 2. The numerical result generated is shown in Fig. 11 and shows good agreement with the analytical solution. However, there are some disturbances when we performed a long time simulation, as shown in Fig. 11. This is because the MTF method cannot transmit *all* the outgoing wave components out of the artificial
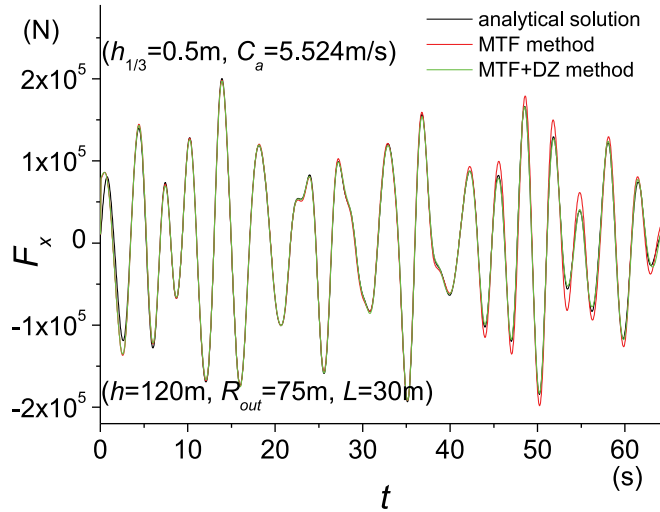
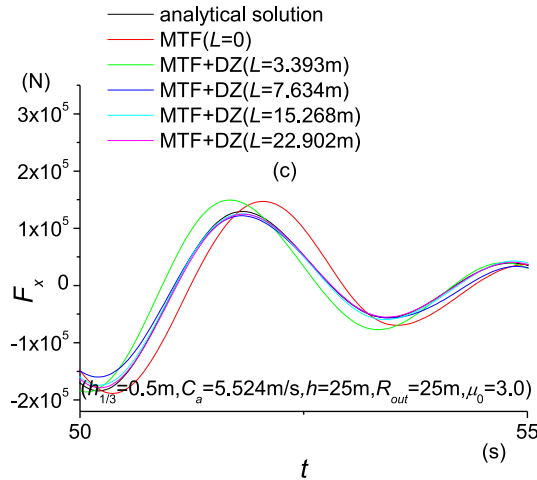**Fig. 12.** Comparison of the MTF method and the hybrid method ($h_{1/3} = 0.5$ m and $\mu_0 = 3.0$).

Fig. 13. Comparison of F_x with different widths of the damping zone ($h_{1/3} = 0.5$ m).

boundary. There are presumably some wave reflections due to the effective range of C_a as described in Fig. 8. (Because of this, we need to explore another radiation condition coupled with the MTF, which will be discussed in Section 3.3.)

3.3. Linear irregular wave diffraction by the hybrid method

As discussed in Sections 3.1 and 3.2, the diffracted waves can effectively propagate away from the fluid domain by the MTF method only when the artificial wave speed C_a is in the prescribed range. Thus, another appropriate radiation condition should be coupled with the MTF on the artificial boundary to minimize the wave reflection when we simulate the irregular wave problem, which includes both high-frequency wave components and low-frequency wave components. Here, we will use a combination of the MTF method and the damping zone method as described in Eqs. (29) and (30).

The calculations are made with the two types of radiation condition (MTF method and hybrid method) imposed, and the results are presented in Fig. 12. It is clear the result has been greatly improved with the hybrid method; and the phenomena of disturbance and reflection have but essentially disappeared.

The relative width of the damping zone with respect to the wavelength should be large enough to minimize the effect of short waves, which cannot be transmitted adequately by the MTF method. The numerical results obtained with different widths of the damping zone are shown in Fig. 13. We can see that it is not necessary to use a large damping zone to eliminate the short wave reflection. In this work, we used $L = 2\pi C_a^2/(2.4^2 g)$ to obtain the necessary width of the damping zone; we found that $L = 2\pi C_a^2/(2.4^2 g)$ suffices for the damping zone, and the results are as expected.
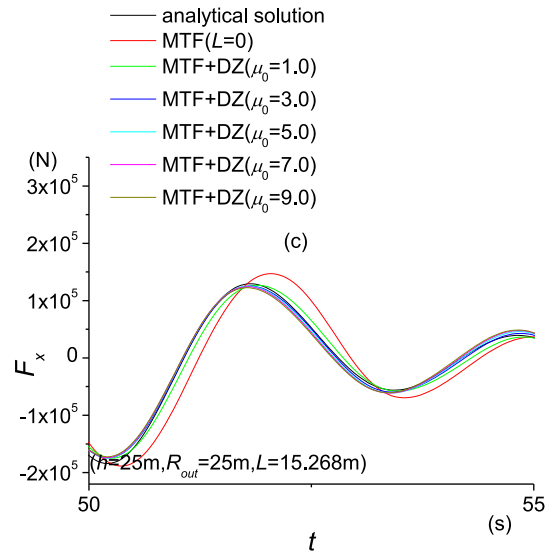
Fig. 14. Comparison of F_x with different strengths of the damping coefficient.

As the role of damping is another critical numerical issue, if the strength of the damping coefficient is too weak or too strong, the outgoing waves may be reflected by the artificial boundary or the inner edge of the damping zone. It is therefore necessary to investigate the sensitivity of the damping zone with regard to the parameters of the damping zone method. The results obtained with different strengths of the damping constant (μ_0) are shown in Fig. 14. It appears that $\mu_0 = 3.0$ is a reasonable choice. Because of this, for the rest of the simulation, we set $\mu_0 = 3.0$.

3.4. Second-order wave diffraction by the MTF method and the hybrid method

To illustrate the numerical model and for comparison with frequency-domain solutions, a bottom-mounted, surface-piercing vertical circular cylinder and a truncated surface-piercing vertical circular cylinder are applied. Before we consider the case of second-order wave–body interaction in an irregular wave, we first undertake a simulation for second-order Stokes wave diffraction of a bottom-mounted cylinder at finite water depth (radius $a = 1$ m, depth $h = a$). Generally, the incident wave and potential are transient. For the periodic Stokes wave at finite water depth, they can be written as:

$$\eta_I = \varepsilon \eta_I^{(1)} + \varepsilon^2 \eta_I^{(2)} = A\cos(kx - \omega t) + \frac{kA^2}{4}\frac{\cosh kh(2 + \cosh 2kh)}{\sinh^3 kh}\cos 2(kx - \omega t), \tag{41}$$

$$\phi_I = \varepsilon \phi_I^{(1)} + \varepsilon^2 \phi_I^{(2)} = \frac{gA}{\omega}\frac{\cosh k(z + h)}{\cosh kh}\sin(kx - \omega t) + \frac{3\omega A^2}{8}\frac{\cosh 2k(z + h)}{\sinh^4 kh}\sin 2(kx - \omega t), \tag{42}$$

where h is the water depth, ω is the wave frequency, and k is the wave number. h, ω, and k are linked by the dispersion equation $\omega^2 = gk\tanh(kh)$.

The amplitude of first-order and second-order forces is given in Figs. 15 and 16, in which the results from Taylor and Hung [2] are also given for comparison. It is seen that the agreement is very good. The time histories of the hydrodynamic force are presented in Fig. 17. We can see that the results are numerically very stable.

Next, the model is applied to the computation of nonlinear forces on a truncated surface-piercing vertical circular cylinder (radius $a = 1$ m, depth $h = 6$ m, draft $d = 1.5$ m). For the periodic Stokes wave at infinite water depth, they can be written as:

$$\phi_I = \varepsilon \phi_I^{(1)} + \varepsilon^2 \phi_I^{(2)} = \frac{gA}{\omega}e^{kz}\sin(kx - \omega t), \tag{43}$$

$$\eta_I = \varepsilon \eta_I^{(1)} + \varepsilon^2 \eta_I^{(2)} = A\cos(kx - \omega t) + \frac{1}{2}A^2 k\cos[2(kx - \omega t)]. \tag{44}$$

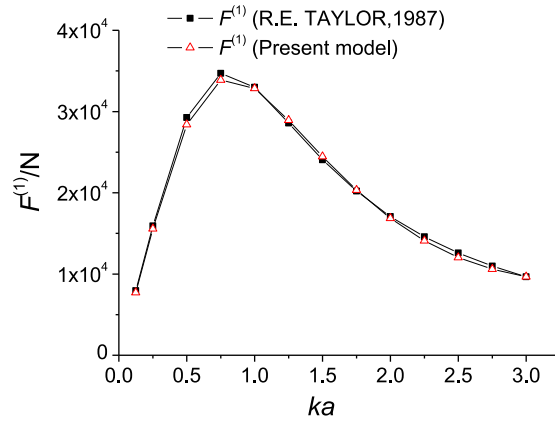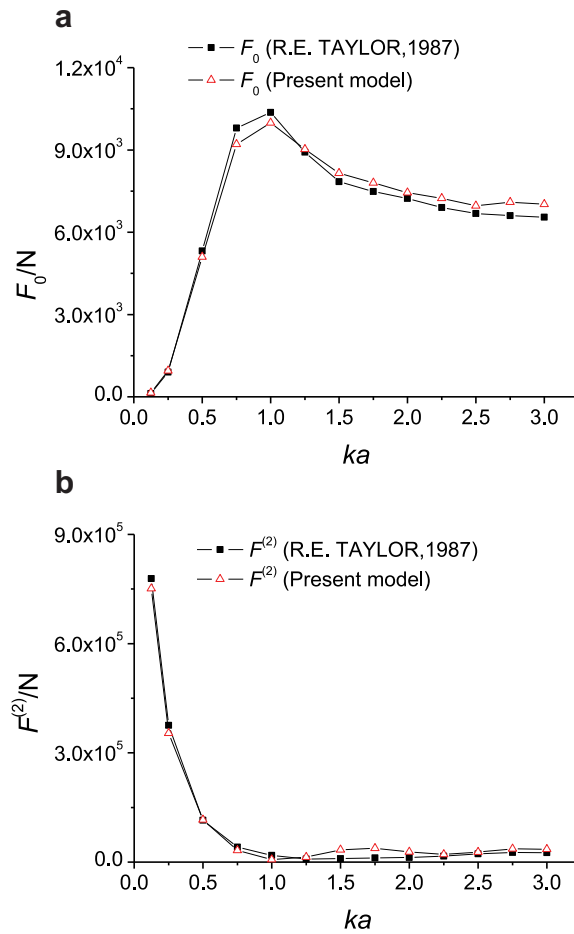**Fig. 15.** The amplitude of the first-order hydrodynamic force versus *ka*.

Fig. 16. The steady force (a) and the amplitude of the second-order double-frequency force (b) versus *ka*.

For irregular incident Stokes waves with M wave components, we have:

$$\phi_{\mathrm{I}}^{(1)} = \sum_{j=1}^{M} \frac{gA_j}{\omega_j} e^{k_j z} \sin(k_j x - \omega_j t), \tag{45}$$

$$\phi_{\mathrm{I}}^{(2)} = \sum_{\omega_j > \omega_l} \sum \omega_j A_j A_l e^{(k_j - k_l)z} \sin\left[(k_j - k_l)x - (\omega_j - \omega_l)\right]. \tag{46}$$
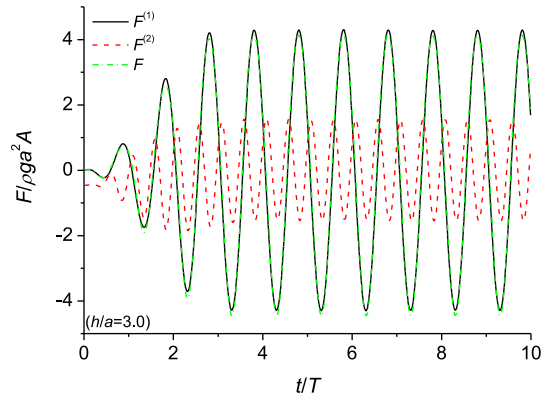
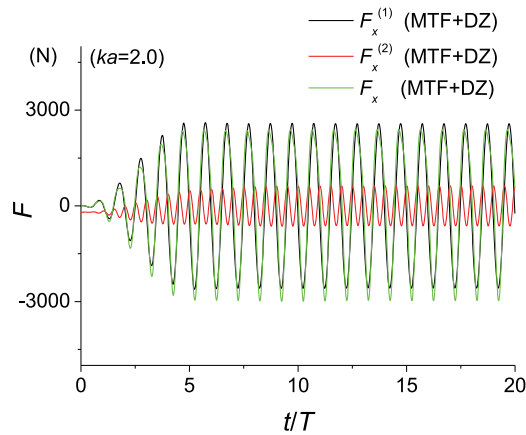**Fig. 17.** Time histories of hydrodynamic force.

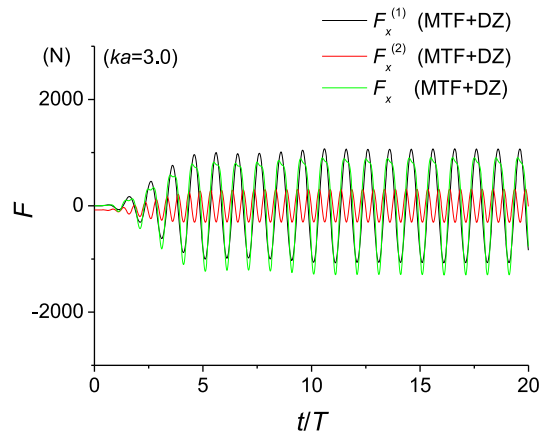**Fig. 18.** Time histories of hydrodynamic force ($ka = 2.0$).

Fig. 19. Time histories of hydrodynamic force ($ka = 3.0$).

Figs. 18–20 show the corresponding time-history hydrodynamic force with $ka = 2$, 3, and 4, respectively. Among them, the nonlinear effect can be found. Here, the artificial wave velocity is set to the corresponding first-order actual wave velocity, and the amplitude A is related to the corresponding first-order wavelength (0.05λ). The numerical results for the irregular wave with three wave components ($ka = 2$, 3, and 4, $M = 3$) are presented in Fig. 21, where the artificial wave velocity is 1.566 m/s and the length of the damping zone is fixed to 2 m. This has been found to give accurate results for long time computation, and same conclusion can be found for the time-domain simulation of low-frequency wave–structure interaction as presented
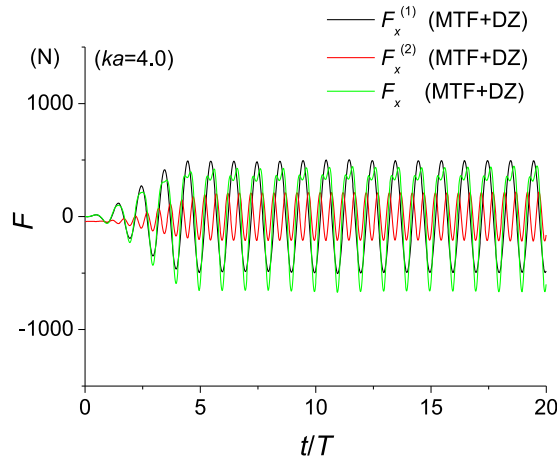
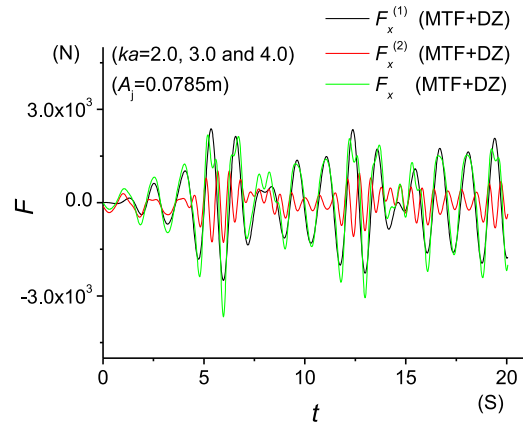**Fig. 20.** Time histories of hydrodynamic force ($ka = 4.0$).

Fig. 21. Time histories of hydrodynamic force with three wave components ($ka = 2.0, 3.0, 4.0$).
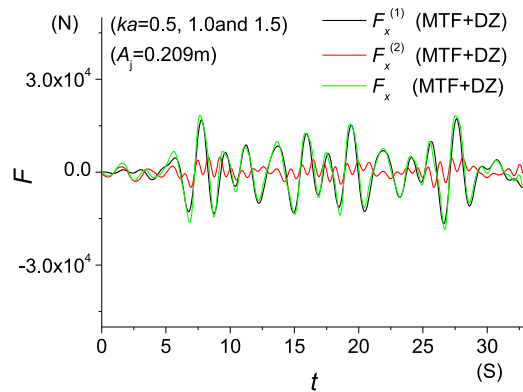

Fig. 22. Time histories of hydrodynamic force with three wave components ($ka = 0.5, 1.0, 1.5$).

in Fig. 22 with three wave components ($ka = 0.5$, 1.0, and 1.5, $M = 3$). We find that the proposed method is applicable to the high-frequency and low-frequency cases, which is very conducive for solving the second-order wave–structure interaction. The calculation also provides an indication that our proposed approach of simulating nonlinear irregular wave–body interaction is feasible and by extension could be used to study the more complex nonlinear irregular random wave–body interaction.

7. Conclusions

A three-dimensional time-domain Rankine panel method has been presented for the solution of the second-order diffraction problem for an irregular wave. An integral form and two auxiliary functions were introduced to update the velocity potential on the free surface. The basic parameters of the MTF method were investigated and the effective range of the additional factor and the artificial wave velocity was obtained. The numerical results show that the MTF method can transmit waves out of a truncated surface efficiently when the artificial wave velocity is taken to be close to the actual wave velocity. However, for the irregular wave simulation, the weak wave reflection from the truncated surface with the MTF method cannot usually be ignored, especially for the nonlinear case; thus, an effective hybrid water wave radiation condition, which is the combination of the MTF and the damping zone, was used and was verified to be excellent. For the second-order (irregular) wave diffraction, the hydrodynamic forces obtained were compared with frequency-domain solutions. The model gave accurate results for both high-frequency and low-frequency wave–structure interaction. The present model can be applied to simulate nonlinear irregular wave–body interaction, and the model is accurate and numerically very stable.

Appendix A. Solution for $\frac{\partial^3 \phi_D^{(1)}(p,t)}{\partial z \partial t^2}$ in Eq. (24)

To avoid use of the difference approximation to evaluate the term $\frac{\partial^3 \phi_D^{(1)}(p,t)}{\partial z \partial t^2}$ in Eq. (24), we used an auxiliary function and set $\psi_1(p, \tau) = \frac{\partial^2 \phi_D^{(1)}(p,\tau)}{\partial \tau^2}$, which satisfies the Laplace equation within the fluid domain,

$$\nabla^2 \psi_1(p, \tau) = 0 \text{ in } \Omega_f^{(0)}, \tag{A.1}$$

and subject to the boundary conditions:

$$\frac{\partial \psi_1(p, \tau)}{\partial n} = \frac{\partial}{\partial n}\left(\frac{\partial^2 \phi_D^{(1)}(p, \tau)}{\partial \tau^2}\right) = \frac{\partial^2}{\partial \tau^2}\left(-M(\tau)\frac{\partial \phi_I^{(1)}(p, \tau)}{\partial n}\right) \text{ on } S_H^{(0)}, \tag{A.2}$$

$$\psi_1(p, \tau) = -g\frac{\partial \phi_D^{(1)}(p, \tau)}{\partial z} \text{ on } S_F, \tag{A.3}$$

$$\frac{\partial \psi_1(p, \tau)}{\partial z} = \frac{\partial}{\partial z}\left(\frac{\partial^2 \phi_D^{(1)}(p, \tau)}{\partial \tau^2}\right) = \frac{\partial^2}{\partial \tau^2}\left(\frac{\partial \phi_D^{(1)}(p, \tau)}{\partial z}\right) = 0 \text{ on } S_B, \tag{A.4}$$

and that ψ_1 satisfies the second-order MTF on the artificial boundary. The Green's function is $G = 1/r_1 + 1/r_2$ for the boundary integral equation.

Appendix B. Solution for $\frac{\partial^2 \phi_D^{(1)}(p,t)}{\partial z^2}$ in Eq. (24)

For the term $\frac{\partial^2 \phi_D^{(1)}(p,t)}{\partial z^2}$ in Eq. (24), we use an auxiliary function too and set $\psi_2(p, \tau) = \frac{\partial \phi_D^{(1)}(p,\tau)}{\partial z}$, which also satisfies the Laplace equation within the fluid domain,

$$\nabla^2 \psi_2(p, \tau) = 0 \text{ in } \Omega_f^{(0)}, \tag{B.1}$$

and subject to the following boundary conditions:

$$\psi_2(p, \tau) = \frac{\partial \phi^{(1)}(p, \tau)}{\partial z} \text{ on } S_H^{(0)}, \tag{B.2}$$

$$\psi_2(p, \tau) = \frac{\partial \phi^{(1)}(p, \tau)}{\partial z} \text{ on } S_F, \tag{B.3}$$

$$\psi_2 = \frac{\partial \phi^{(1)}(p, \tau)}{\partial z} = 0 \text{ on } S_B, \tag{B.4}$$

$$\psi_2(p, \tau) = \frac{\partial \phi^{(1)}(p, \tau)}{\partial z} \text{ on } S_C, \tag{B.5}$$

Here, however, the Green's function is $G = 1/r_1 - 1/r_2$ for the boundary integral equation.

References

[1] B. Molin, Second order diffraction loads upon three dimensional bodies, Appl. Ocean Res. 1 (1979) 197–202.
[2] R.E. Taylor, S.M. Hung, Second order diffraction forces on a vertical cylinder in regular waves, Appl. Ocean Res. 9 (1987) 19–30.
[3] M.H. Kim, D.K.P. Yue, The complete second-order diffraction waves around an axisymmetric body. Part 1. Monochromatic incident waves, J. Fluid Mech. 200 (1989) 235–262.
[4] M. Isaacson, K.F. Cheung, Time-domain second-order wave diffraction in three dimensions, J. Waterw. Port Coast. Ocean Eng. 118 (1992) 496–516.
[5] M. Isaacson, J.Y.T. Ng, K.F. Cheung, Second-order wave radiation of three-dimensional bodies by time-domain method, Int. J. Offshore Polar Eng. 3 (1993) 264–272.
[6] J.N. Newman, The second-order wave force on a vertical cylinder, J. Fluid Mech. 320 (1996) 417–443.
[7] C.Z. Wang, G.X. Wu, Time domain analysis of second-order wave diffraction by an array of vertical cylinders, J. Fluids Struct. 23 (2007) 605–631.
[8] J.N. Newman, Analysis of wave generators and absorbers in basins, Appl. Ocean Res. 32 (2010) 71–82.
[9] I. Orlanski, A simple boundary condition for unbounded hyperbolic flows, J. Comput. Phys. 21 (1976) 251–269.
[10] M. Israeli, S.A. Orszag, Approximation of radiation boundary conditions, J. Comput. Phys. 41 (1981) 115–135.
[11] G.Z. Forristall, Irregular wave kinematics from a kinematic boundary condition fit (KBCF), Appl. Ocean Res. 7 (1985) 202–212.
[12] A. Clément, Coupling of two absorbing boundary conditions for 2D time-domain simulations of free surface gravity waves, J. Comput. Phys. 126 (1996) 139–151.
[13] S.Y. Boo, Linear and nonlinear irregular waves and forces in a numerical wave tank, Ocean Eng. 29 (2002) 475–493.
[14] D. Clamond, D. Fructus, J. Grue, Ø. Kristiansen, An efficient model for three-dimensional surface wave simulations. Part II: generation and absorption, J. Comput. Phys. 205 (2005) 686–705.
[15] Z.P. Liao, Extrapolation nonreflecting boundary conditions, Wave Motion 24 (1996) 117–138.
[16] Z.P. Liao, Introduction to Wave Motion Theories for Engineering, Science Press, Beijing, China, 2002 (in Chinese).
[17] C.W. Zhang, W.Y. Duan, Numerical study on a hybrid water wave radiation condition by a 3D boundary element method, Wave Motion 49 (5) (2012) 525–543.
[18] G. Xu, Time-domain Simulation of Second-Order Hydrodynamic Force on Floating Bodies in Irregular Waves, Doctor of Engineering (in Chinese), Harbin University, Harbin, China, 2009.
[19] W.Y. Duan, T.Y. Zhang, Non-reflecting simulation for fully-nonlinear irregular wave radiation, in: Proceedings of the 24th International Workshop on Water Wave and Floating Bodies, Russia, 2009.
[20] G. Xu, W.Y. Duan, Second-order hydrodynamic analysis of surface-piercing circular cylinders undergoing heave motion, J. Harbin Eng. Univ. 31 (2010) 414–420 (in Chinese).
[21] G. Xu, W.Y. Duan, Numerical investigation on second-order wave diffraction based on Rankine source method, J. Harbin Eng. Univ. 31 (2010) 1144–1152 (in Chinese).
[22] G. Xu, W.Y. Duan, Time domain simulation for water wave radiation by floating structures (part A), J. Mar. Sci. Appl. 7 (2008) 226–235.
[23] G. Xu, W.Y. Duan, Time-domain simulation of hydrodynamic force on semi-submersible platform in regular wave excitation, J. Jiangsu Univ. Sci. Technol. 26 (2012) 1–7 (Natural Science Edition).
[24] G. Xu, W.Y. Duan, Time domain simulation of irregular wave diffraction, in: Proceedings of the 8th International Conference on Hydrodynamics, Nantes, France, 2008.
[25] G. Xu, A.M.S. Hamouda, Time-domain simulation of second-order wave diffraction in irregular wave, in: Proceedings of the ASME 2012 31st International Conference on Ocean, Offshore and Arctic Engineering, Rio de Janeiro, Brazil, 2012.
[26] Y.S. Dai, W.Y. Duan, Potential Flow Theory of Ship Motions in Waves, National Defence Industry Press, Beijing, China, 2008 (in Chinese).
[27] P.D. Sclavounos, D.E. Nakos, Stability analysis of panel methods for free surface flows with forward speed, in: Proceedings of the 17th Symposium on Naval Hydrodynamics, Netherlands, 1993.
[28] Y.S. Dai, Potential Flow Theory of Ship Motions in Waves in Frequency and Time Domain, National Defence Industry Press, Beijing, China, 1998 (in Chinese).